WRF Dynamical Downscaling and Bias Correction Schemes for NCEP Estimated Hydro-Meteorological Variables

Prashant K. Srivastava · Tanvir Islam · Manika Gupta · George Petropoulos · Qiang Dai

Abstract Rainfall and Reference Evapotranspiration (ETo) are the most fundamental and significant variables in hydrological modelling. However, these variables are generally not available over ungauged catchments. ETo estimation usually needs measurements of weather variables such as wind speed, air temperature, solar radiation and dew point. After the development of reanalysis global datasets such as the National Centre for Environmental Prediction (NCEP) and high performance modelling framework Weather Research and Forecasting (WRF) model, it is now possible to estimate the rainfall and ETo for any coordinates. In this study, the WRF modelling system was employed to downscale the global NCEP reanalysis datasets over the Brue catchment, England, U.K. After downscaling, two statistical bias correction schemes were used, the first was based on sophisticated computing algorithms i.e., Relevance Vector Machine (RVM), while the second was based on the more simple

P. K. Srivastava (✉) · M. Gupta
Hydrological Sciences, NASA Goddard Space Flight Center, Greenbelt, MD, USA
e-mail: prashant.k.srivastava@nasa.gov

Prashant K. Srivastava
e-mail: prashant.just@gmail.com

P. K. Srivastava
Earth System Science Interdisciplinary Center, University of Maryland, College Park, MD, USA

T. Islam
NOAA/NESDIS Center for Satellite Applications and Research, Greenbelt, MD, USA

T. Islam
Cooperative Institute for Research in the Atmosphere, Colorado State University, Fort Collins, CO, USA

G. Petropoulos
Department of Geography and Earth Sciences, University of Aberystwyth, Wales, UK

Q. Dai
Department of Civil Engineering, University of Bristol, Bristol, UK

M. Gupta
Universities Space Research Association, Columbia, MD, USA

Generalized Linear Model (GLM). The statistical performance indices for bias correction such as *%Bias*, index of agreement (*d*), Root Mean Square Error (*RMSE*), and Correlation (*r*) indicated that the RVM model, on the whole, displayed a more accomplished bias correction of the variability of rainfall and ETo in comparison to the GLM. The study provides important information on the performance of WRF derived hydro-meteorological variables using NCEP global reanalysis datasets and statistical bias correction schemes which can be used in numerous hydro-meteorological applications.

Keywords Hydro-meteorological variables · Weather research and forecasting model · WRF downscaling · RVM, GLM, Bias correction

1 Introduction

Numerical weather prediction (NWP) is a technique used to forecast weather variables by solving numerical and physical models (Ritter and Geleyn 1992). Over the last few decades, a numbers of studies have examined the development of NWP modeling and their subsequent application (Gutman and Ignatov 1998; Ishak et al. 2014; Lorenc 1986). One such model is the Mesoscale model Version 5 (MM5) (Grell et al. 1994), which was developed by the National Center for Atmospheric Research (NCAR) in the United States. After its successful application, an advanced version of the model i.e., the Weather Research Forecast (WRF) model was released to the research community (Skamarock et al. 2005). After its release, and due to the high versatility of the WRF model, a number of studies have utilized this advanced model in research related to wide range of atmospheric phenomena, producing meteorological variables, hydrological modeling, weather research, climate monitoring and change, flood forecasting and water resource management amongst others (Borge et al. 2008; Chen et al. 2011; Ishak et al. 2013; Islam et al. 2013; Price et al. 2012; Srivastava et al. 2013b, 2014a). Aside from its use as a stand-alone NWP model, the WRF model can also be used with global reanalysis datasets, such as those available from the National Centre for Environmental Prediction (NCEP) and the European Center for Medium range Weather Forecasting (ECMWF). Notably, these global datasets have coarse horizontal resolutions and need downscaling to provide information at finer resolution using models like WRF/MM5 (Caldwell et al. 2009; Heikkilä et al. 2011; Lo et al. 2008). This downscaling is required to provide high resolution meteorological datasets such as wind speed, air temperature, solar radiation, dew point and rainfall suitable for regional or local uses (Srivastava et al. 2013d, 2014b).

The hydrological processes of any basins are influenced by hydro-meteorological variables, thus changes in such variables have implications on water resources (Liolios et al. 2014; Srivastava et al. 2013c). The major weather input variables influencing the estimation of Reference Evapotranspiration (ETo) includes wind speed, air temperature, dew point and solar radiation (Allen et al. 1998). The mesoscale model downscaled weather variables could potentially be used for ETo estimation, especially in ungauged catchments (Srivastava 2013). Similarly, rainfall is also one of the fundamental variables of the Earth's hydrological cycle (Bringi et al. 2011; Islam et al. 2012b). It is an important parameter required for climate and hydrological forecasting and hence its accurate measurements are crucial for the hydrological community (Ishak et al. 2014; Islam et al. 2012a; Petropoulos et al. 2013).

Piani et al. in (2010a) showed that mesoscale model derived ETo and precipitation can be used with hydrological models after statistical bias correction to provide a more realistic datasets for hydro-meteorological applications (Piani et al. 2010b). Bias correction can be done in a number of ways, amongst which, computational intelligence techniques are the most

popular among users (Islam et al. 2014). Bias correction using simple algorithms like the Generalized Linear Models (GLM) are easily applicable and least computationally demanding (Schoof and Pryor 2001; Trigo and Palutikof 2001; Weichert and Bürger 1998). Another technique is Relevance Vector Machines (RVMs), which are powerful mathematical tools used for non-linear analysis and have been applied successfully for hydro-meteorological studies (Abrahart and See 2007; Hong et al. 2004). Other potential tools which can be used for bias correction is Support Vector Machines (SVMs); however, SVMs has some drawbacks such as rapid increase of basis functions with the size of training data set and an absence of probabilistic interpretation (Srivastava et al. 2013a). To overcome these problems, a sparse Bayesian probabilistic learning framework based Relevance Vector machine (RVM) has been developed by Tipping (2001). Hence, instead of SVMs, RVM is used in this study.

In this study, the WRF model has been applied and tested over the Brue catchment, England, UK. for deriving ETo and rainfall using the global NCEP reanalysis datasets. However, before using modeled data for any application, a brief analysis of products are required for its efficiency in comparison to the observed datasets. Furthermore, before obtaining practical outputs from such models, statistical bias correction is needed. In purview of the above mentioned problems, the main aim of this research focuses on the following objectives: (1) Simulation of hydro-meteorological variables using the state of the art WRF mesoscale model and global NCEP reanalysis datasets, (2) Estimation of the seasonality pattern in the WRF estimated ETo and rainfall datasets, and (3) Assessment of the performance of GLM and RVM for bias correction using the data derived from the WRF model and the ground based station datasets.

This paper has the following structure. In Section 2, we detail the study area, data sets, WRF modeling systems, bias correction algorithms such as RVMs and GLM, equation for ETo and performance statistics. Section 3 presents the results of the performance of the approaches utilized and subsequently discusses these results. Section 4 gives final remarks and conclusions of this work.

2 Materials and Methodology

2.1 Study Area

The Brue catchment is located in the south-west of England, with central coordinates of 51.11° N and 2.47° W. The geographical location of the study area is shown in Fig. 1. The meteorological datasets are provided by the British Atmospheric Data Centre (BADC), UK, including wind, net radiation, surface temperature and dew point for the period from June 2010 to November 2011. The data provided by BADC is used for evaluating the hourly downscaled meteorological data from the WRF model. The global NCEP (National Centers for Environmental Prediction) reanalysis data used in this study with WRF can be downloaded from their respective websites (http://rda.ucar.edu/). The main purposes of reanalysis data such as NCEP/NCAR are to deliver compatible, high-resolution and high quality historical global atmospheric datasets for use by the weather research community. The resolutions of these data are 1° × 1° in space and 6 h in time. Hourly datasets from the first 12 months June 2010 to May 2011 were used for training, and the remaining 6 months (June 2011-Nov2011) for validation purposes.

2.2 Weather Research and Forecasting (WRF) Model

The model employed for this study is the WRF model (version 3.1.1). The WRF model has a rapidly growing user community and has been used for numerous hydro-meteorological and
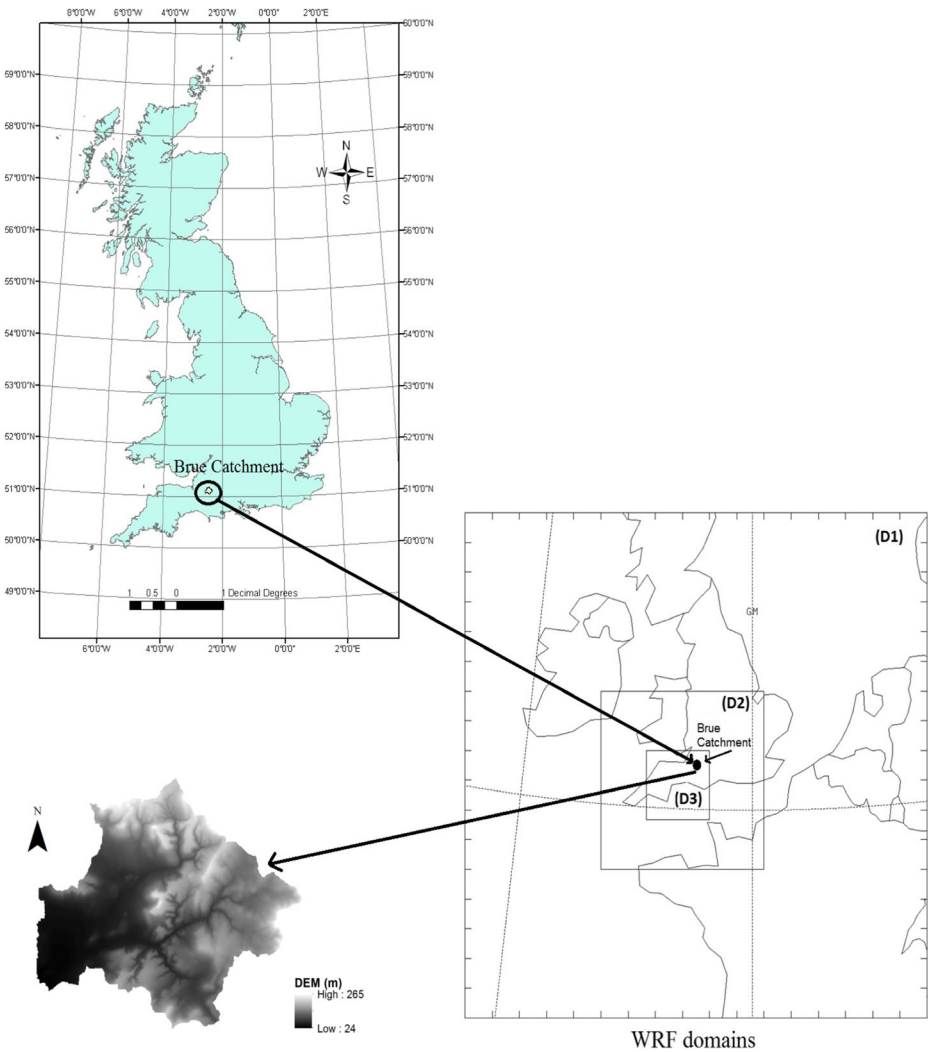
Fig. 1 WRF domains employed in this study with catchment location

operational weather forecasting studies amongst others (Borge et al. 2008; Chen et al. 2011; Draxl et al. 2010; Heikkila et al. 2011). The WRF model is centered over the Brue catchment with three nested domains (D1, D2 and D3) of horizontal grid spacing of 81, 27 and 9 km, out of which the finest resolution innermost domain (D3) is used in this study (Fig. 1). A two-way nesting scheme is used which allows information from the child domain to be fed back to the parent domain. Imposed boundary conditions are updated every 6 h using the National Centers for Environmental Prediction (NCEP) Final Analysis (1°×1° FNL) data set. The WRF model is used to downscale the NCEP data to produce wind, solar radiation, surface temperature, dew point temperature and rainfall. After downscaling, the ETo was estimated using the Penmen and Monteith equation discussed in section 2.5.

The main physical options included the WRF Dudhia shortwave radiation (Dudhia 1989) and Rapid Radiative Transfer Model (RRTM) long wave radiation (Mlawer et al. 1997) with

Lin microphysical parameterization; the Betts-Miller-Janjic Cumulus parameterisation schemes; and the Yonsei University (YSU) planetary boundary layer (PBL) scheme (Hu et al. 2010). The Betts-Miller-Janjic Cumulus parameterization scheme was used because it is well tested for regional application and precipitation forecasting (Vaidya and Singh, 2000). Gilliland and Rowe (2007) found that it considers a sophisticated cloud mixing scheme in order to determine entrainment/detrainment which is found to be more suitable for non-tropical convection. The Arakawa C-grid was used for the horizontal grid distribution. The 3rd-order Runge–Kutta was used for time integration as it is stable without any damping (Zhong 1996), while the 6th-order centered differencing scheme was used as the spatial differencing scheme. The reason behind using this differencing scheme was its high numerical stability. The brief analysis by Chu and Fan (1997) indicated that the 6th-order scheme has error reductions by factors of 5 compared to the fourth-order difference scheme, and by factors of 50 compared to the second-order difference scheme. The Thermal diffusion scheme was used for the surface layer parameterization. The top and bottom boundary condition chosen for the study were Gravity wave absorbing (diffusion or Rayleigh damping) and Physical or free-slip respectively. The Lambert conformal conic projection was used as the model horizontal coordinates. The vertical coordinate η is defined as:

$$\eta = \frac{(p_r - p_t)}{(p_{rs} - p_t)} \tag{1}$$

where, p_r is pressure at the model surface being calculated; p_{rs} is the pressure at the surface and p_t is the pressure at the top of the model.

2.3 Relevance Vector Machine

Tipping (2001) proposed the relevance vector machine (RVM) in a Bayesian context. It is based on a probabilistic theory operated by a set of hyperparameters associated with weights iteratively estimated from the data. RVM typically utilizes fewer kernel functions and the training vectors associated with nonzero weights are called relevance vectors. The RVM model variable can be characterized for forecast y at a given x by the Eqs. (2) and (3):

$$y = f(x) + \varepsilon_n \ where \ \varepsilon_n \tilde{} N\left(0, \sigma_{\varepsilon_n}^2\right) \tag{2}$$

$$p\left(y \middle| w, \sigma_{\varepsilon_n}^2\right) = \left(2\pi\sigma_{\varepsilon_n}^2\right)^{-l\big/2} \exp\left\{-\frac{1}{2\sigma_{\varepsilon_n}^2} \|y - \Phi_w\|^2\right\} \tag{3}$$

where, weights, $w = (w_0, w_1, \ldots, w_l)^T$, $\sigma_{\varepsilon_n}^2$ is noise variance, εn are independent samples from some noise process and $\Phi_{(x_i)} = [1, K(x_i, x_1), K(x_i, x_2), \ldots, K(x_i, x_l)]^T$ in which $K \ (xi, \ xl)$ represents kernel function.

Tipping (2001) recommended the addition of a complex penalty to the likelihood or error function to avoid the over fitting problem of w and $\sigma_{\varepsilon_n}^2$. The higher-level hyperparameters are used to constrain an explicit zero-mean Gaussian prior probability distribution over w (Ghosh and Mujumdar 2008):

$$p(w|\alpha) = \prod_{i=0}^{l} N\left(w_i \middle| 0, \alpha_i^{-1}\right) \tag{4}$$

where α is a hyperparameter vector. The posterior overall unknowns could be computed following the Bayesian rule:

$$p\left(w, \alpha, \sigma_{\varepsilon_n}^2 | y\right) = \frac{p\left(y | w, \alpha, \sigma_{\varepsilon_n}^2\right) \cdot p\left(w, \alpha, \sigma_{\varepsilon_n}^2\right)}{\int p\left(y | w, \alpha, \sigma_{\varepsilon_n}^2\right) p\left(w, \alpha, \sigma_{\varepsilon_n}^2\right) dw d\alpha d\sigma_{\varepsilon_n}^2} \tag{5}$$

Computation of $p\left(w, \alpha, \sigma_{\varepsilon_n}^2 | y\right)$ in Eq. (5) can be decomposed as:

$$p\left(w, \alpha, \sigma_{\varepsilon_n}^2 | y\right) = p\left(w | y, \alpha, \sigma_{\varepsilon_n}^2\right) p\left(\alpha, \sigma_{\varepsilon_n}^2 | y\right) \tag{6}$$

While the posterior distribution of the weight can be given by

$$p\left(w | y, \alpha, \sigma_{\varepsilon_n}^2\right) = \frac{p\left(y | w, \sigma_{\varepsilon_n}^2\right) \cdot p(w | \alpha)}{p\left(y | \alpha, \sigma_{\varepsilon_n}^2\right)} = (2\pi)^{-l/2} |\Sigma|^{-1/2}$$

$$\times \exp\left\{-\frac{1}{2}(w-\mu)^T \Sigma^{-1}(w-\mu)\right\} \tag{7}$$

where the posterior covariance and mean are respectively:

$$\Sigma = \left(\sigma_{\varepsilon_n}^{-2} \Phi^T \Phi + A\right)^{-1} \tag{8}$$

$$\mu = \sigma_{\varepsilon_n}^{-2} \Sigma \Phi^T y \tag{9}$$

where, $A = diag(\alpha_0, \ldots, \alpha_l)$.

Therefore, the machine learning becomes a search for the hyperparameter posterior most probable, i.e., the maximization of $p\left(\alpha, \sigma_{\varepsilon_n}^2 | y\right) \propto p\left(y | \alpha, \sigma_{\varepsilon_n}^2\right) p(\alpha) p\left(\sigma_{\varepsilon_n}^2\right)$ with respect to α and $\sigma_{\varepsilon_n}^2$. For uniform hyperpriors, it is required to maximize the term $p\left(y | \alpha, \sigma_{\varepsilon_n}^2\right)$, which is computable and given by:

$$p\left(y | \alpha, \sigma_{\varepsilon_n}^2\right) = \int \frac{p\left(y | w, \sigma_{\varepsilon_n}^2\right) p(w | \alpha) dw = (2\pi)^{-l/2} |\sigma_{\varepsilon_n}^2 I + \Phi A^{-1} \Phi^T|^{1/2}}{\times \exp\left\{-\frac{1}{2}(y)^T \left(\sigma_{\varepsilon_n}^2 I + \Phi A^{-1} \Phi^T\right)^{-1}(y)\right\}} \tag{10}$$

At convergence of the hyperparameter estimation procedure, predictions can be made based on the posterior distribution over the weights, conditioned on the maximized most probable values of α and $\sigma_{\varepsilon_n}^2$, α_{MP} and σ_{MP}^2 respectively. The predictive distribution for a given y^* can be computed using:

$$p(y_* | y, \alpha_{MP}, \sigma_{MP}^2) = \int p(y_* | w, \sigma_{MP}^2) p(w | y, \alpha_{MP}, \sigma_{MP}^2) dw \tag{11}$$

Since both terms in the integrand are Gaussian, this can be readily computed, giving:

$$p(y_* | y, \alpha_{MP}, \sigma_{MP}^2) = N(y_* | t_*, \sigma_*^2) \tag{12}$$

where $t_* = \mu^T \Phi(x_*)$ and $\sigma_*^2 = \sigma_{MP}^2 + \Phi(x_*)^T \Sigma \Phi(x_*)$.

The RVM predictions are probabilistic and it doesn't make unnecessarily liberal use of basis functions like SVMs. Use of a fully probabilistic framework is a useful approach in RVMs with a priori over the model weights governed by a set of hyperparameters.

2.4 Generalized Linear Model (GLM)

Generally, in linear regression, the relationships between two variables are obtained by fitting a linear equation to observed data (Srivastava et al. 2014d). One variable is considered to be an explanatory variable (x_i), and the other is considered to be a dependent variable (y_i) (Johnson and Wichern 2002). By considering the familiar linear regression model:

$$y_i = x_i b + e_i, \tag{13}$$

where $i = 1, \ldots, n,; y_i$ is a dependent variable; x_i is a vector of k independent predictors; b is a vector of unknown parameters; and the e_i is stochastic disturbances. The Generalized Linear Model (GLM) is a flexible generalization of ordinary linear regression that allows for response variables that have error distribution models other than a normal distribution. The GLM model is characterized by stochastic component, systematic component and link between the random and systematic components (McCullagh and Nelder 1989). The GLM generalizes linear regression by allowing the linear model to be related to the response variable via a link function and by allowing the magnitude of the variance of each measurement to be a function of its predicted value.

2.5 ETo Estimation Using FAO56 Penman and Monteith (PM) Method

The ETo from WRF downscaled and measured meteorological variables was calculated using the Penman and Monteith (PM) method (Monteith 1965; Penman 1956). A comprehensive overview of the PM method is provided in the FAO56 report (Allen et al. 1998). The FAO Penman-Monteith method is recommended as the sole ETo method for determining reference evapotranspiration. The ETo (in mm/hr) according to the PM equation is as follows:

$$ETo = \frac{0.408 \Delta (R_n - G) + \gamma \dfrac{37}{T + 273} U_2 (e_s - e_a)}{\Delta + \gamma \left(1 + \dfrac{r_c}{r_a}\right)} \tag{14}$$

where Δ = slope of the saturated vapour pressure curve (kPa/°C); R_n = net radiation at the crop surface (MJ/m^2/hr); G = soil heat flux density (MJ/m^2/hr); γ = psychrometric constant (kPa/°C); T = mean air temperature at 2 m height (°C); e_s = saturation vapour pressure (kPa); e_a = actual vapour pressure (kPa); $e_s - e_a$ = saturation vapour pressure deficit (kPa); U_2 = wind speed at 2 m height (m/s); r_a (aerodynamic resistance) = 208/ U_2 s m^{-1}; and r_c (canopy resistance) = 70 s m^{-1}.

2.6 Statistical Parameters

In this study we compared the WRF downscaled and bias corrected values of meteorological variables with the data provided by *BADC*. Although there are many statistics available, six of them are used in this study: *root mean square error (RMSE), Index of Agreement (d)* (Willmott

et al. 1985), *Standard Deviation (SD), MAE, %Bias and Correlation (r)*. Root Mean Square Error (RMSE) is represented through Eq. (15),

$$RMSE = \sqrt{\left(\frac{1}{n}\sum_{i-1}^{n}[y_i - x_i]^2\right)} \tag{15}$$

Mean Absolute Error (*MAE*) (Eq.16),

$$MAE = \frac{1}{n}\sum_{j=1}^{n}\left|y_{(ij)} - x_j\right| \tag{16}$$

Correlation (*r*) (Eq.17),

$$r = \frac{n\sum xy - \left(\sum x\right)\left(\sum y\right)}{\sqrt{n\left(\sum x^2\right) - \left(\sum x\right)^2}\sqrt{n\left(\sum y^2\right) - \left(\sum y\right)^2}} \tag{17}$$

Percent bias *(%Bias)* measures the deviation of the simulated values from the observed ones. The optimal value of *%Bias* is 0.0, with low-magnitude values indicating satisfactory model simulation (Eq. 18).

$$\%Bias = 100*\left[\sum (y_i - x_i) \Big/ \sum (x_i)\right] \tag{18}$$

The index of agreement (d) was proposed by (Legates and McCabe 1999; Willmott et al. 1985) to overcome the insensitivity of NSE to differences in the observed and predicted means and variances. The index of agreement represents the ratio of the mean square error and the potential error (Willmott et al. 1985) and is defined as Eq. (19):

$$d = 1 - \frac{\sum_{i=1}^{n}(x_i - y_i)^2}{\sum_{i=1}^{n}\left(\left|y_i - x^-\right| + \left|x_i - x^-\right|\right)^2} \tag{19}$$

where *n* is the number of observations; x_i is the ground based measurements and y_i is the estimated measurements; $\bar{x}$ is the mean of ground based measurements.

3 Results and Discussion

3.1 Evaluation of Meteorological Variables Estimated from WRF

Downscaling is very important for obtaining high resolution hydro-meteorological datasets. It is a technique that provides the estimates of local weather variables at sub-grid scales from the coarser global reanalysis datasets such as NCEP to a finer resolution. In this work, the WRF downscaled estimated hydro-meteorological parameters were used for all the subsequent analysis, with domain 3 as an area of interest (Fig. 1). To evaluate the data derived from the WRF downscaled weather variables and the in-situ measurements, three statistical metrics, namely the *MAE*, *RMSE* and *r* were derived. The relative time series for all the variables

downscaled using the WRF modelling system are presented in Fig. 2, while the performance statistics of the weather variables are provided in Table 1. The modelled surface temperature was generally greater than the measured. The downscaled temperature exhibited a good correlation with the observed and simulated temperature ($r=0.74$). From the error statistics, surface temperature was found to have the third lowest error in the group and very small *MAE* (i.e., the model overestimates in comparison with the measured value). The *MAE* (3.84 °C) and *RMSE* (4.95 °C) showed a reasonable value for the global data. Solar radiation was the most difficult variable to downscale with significant overestimation. However, in this study, WRF downscaled solar radiation indicated a good correlation of 0.80, *MAE* (66.96 Watt/m^2) and *RMSE* (133.10 Watt/m^2) with the observed datasets. According to Allen *et al.* (1998), net solar

(a)

(b)
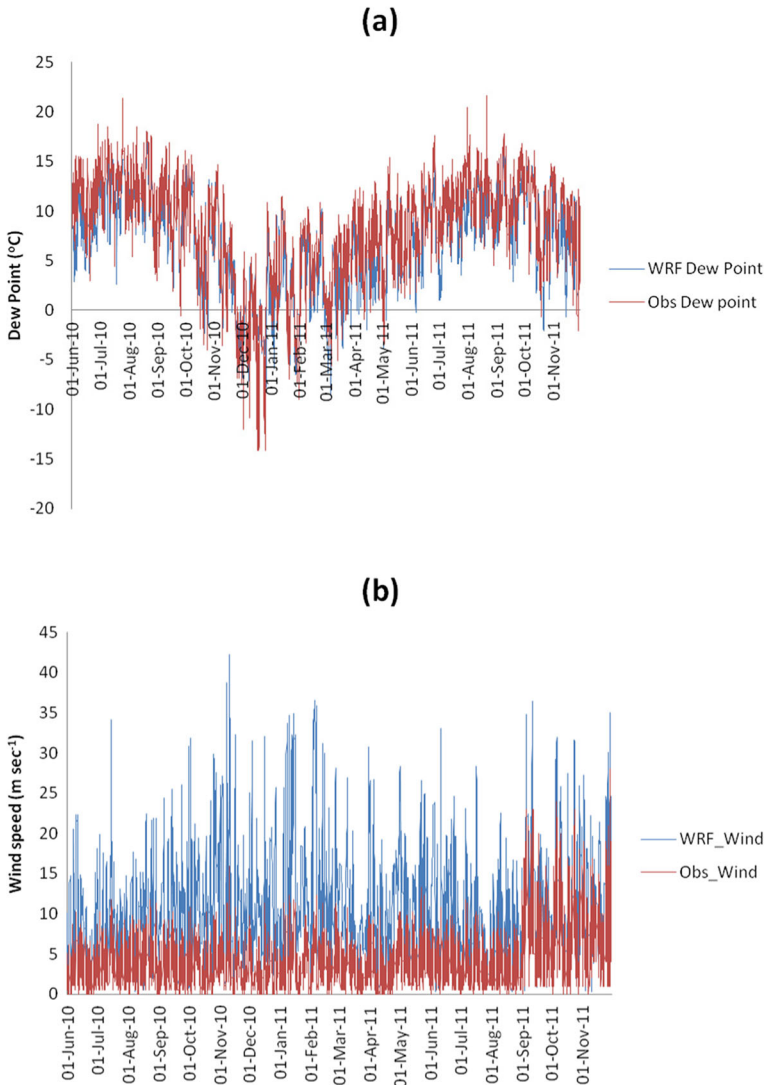
Fig. 2 (**a-d**) Time series plots of the meteorological variables under consideration
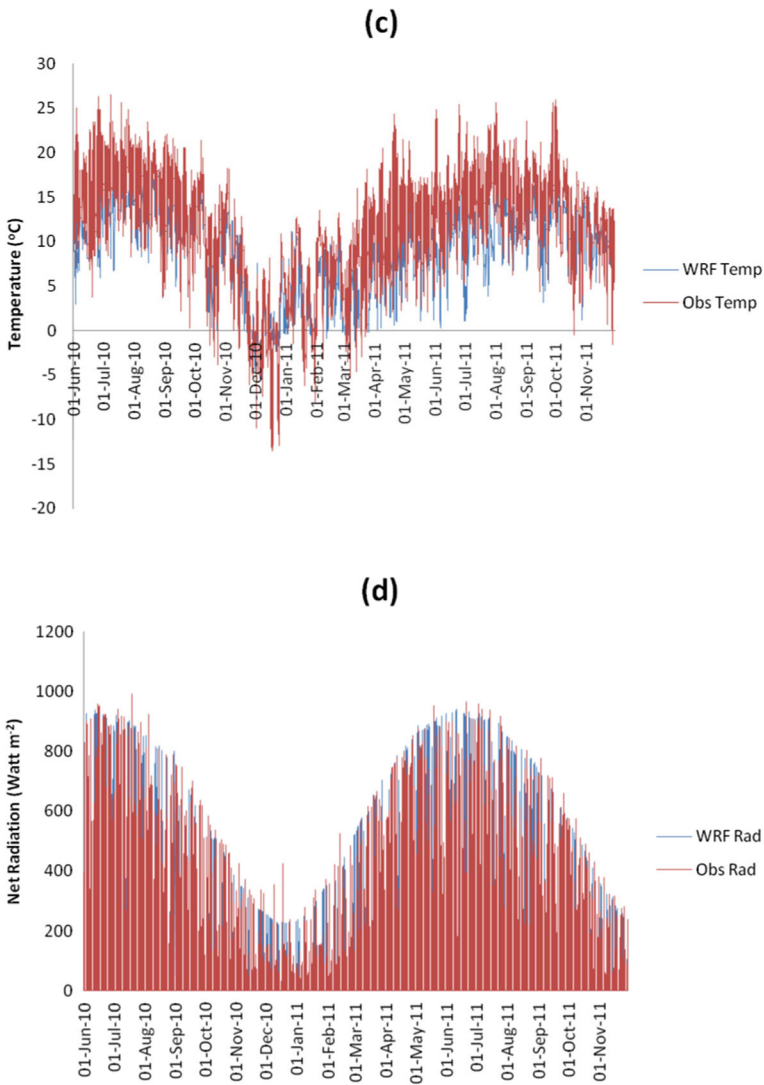
Fig. 2 (continued)

radiation is the balance of incoming solar radiation and outgoing terrestrial radiation, which varies with seasons, which could be a possible reason for the high error. The wind speeds from

Table 1 Performance Statistics of the data estimated using WRF downscaling in comparison to the ground observations

Variable	MAE	RMSE	Correlation
Temperature (°C)	3.84	4.95	0.74
Wind (m/sec)	6.75	8.37	0.57
Net radiation (Watt/m^2)	66.96	133.1	0.80
Dew point (°C)	2.16	2.85	0.88

the model and observation datasets revealed comparable patterns, however the downscaled wind speed values were significantly greater than the observed (*MAE*=6.75 m/sec; *RMSE*= 8.37 m/sec) with correlation of 0.57. Errors of the same kind in overestimated wind speed were also reported by Hanna and Yang (2001). The reason for this large discrepancy is possibly due to the sensitivity of wind to local environmental conditions. Along with temperature, dew point is considered as an important weather element which affects the reference ETo of a region (Mahmood and Hubbard 2005). Dew point in the series had the highest correlation of 0.88, lowest *RMSE* of 2.85 °C and *MAE* of 2.16 °C as compared to the observed datasets.

3.2 Seasonal Analysis of WRF ET and Rainfall Products with Observed Datasets

This approach represents a more direct comparison between the hydro-meteorological variables with the observed station based datasets and rain gauge information. The time series obtained for ETo and rainfall are shown in Fig. 3. The pattern in ETo derived from WRF
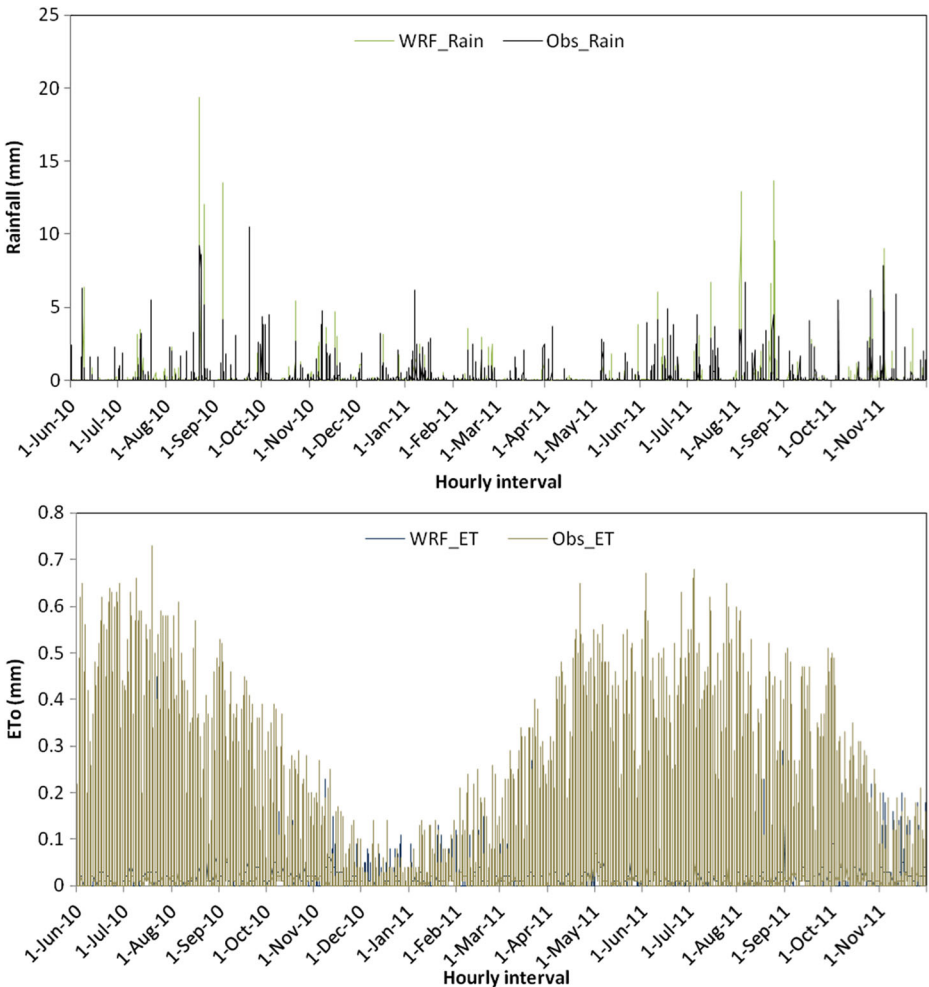

Fig. 3 Seasonal variations in observed and WRF estimated ETo and rainfall

variables indicated a closer relationship with the observed station based datasets. The ETo content was higher in mid-April and August, corresponding to the dry season during the time period under study. Generally, ETo and rainfall showed marked fluctuations over the entire period with rapid and sharp responses. The comparison between ETo and rainfall exhibited a high variability with season, and followed a strong seasonal cycle. The increase in ETo can be attributed to the increasing temperature, with high evaporative demands through the April-May and August-September periods leading to a progressive drying of the soil. The rainfall pattern showed that the period between March to May was slightly drier than other months, while November-December was generally the wettest period. Generally air temperature was low over winter, and soils were near to the field capacity until mid-April, where it subsequently increased for the remaining months. Increasing air temperature after mid- April or May can lead to a substantial ETo development. Interestingly, the solar radiation values were also high during the period from April to mid- August, revealing the strong influence exerted by solar radiation conditions on both surface and subsurface response. It was observed that during the dry conditions, ETo and rainfall displayed nearly similar trends.

3.3 Bias Correction Schemes and Parameterization

3.3.1 Parameterization of GLM and RVM

The GLM model used in this study was comprised of the WRF parameters as explanatory variables and the observed dataset as a dependent variable. The binomial regression family has been used with probit as a link function and binomial as a variance. The RVM technique needs to be optimised for its parameters for a satisfactory result. A preliminary analysis of parameters was performed before using it for bias correction following the method given by Srivastava et al. in (2013a). The model selection of RVM was based on subsuming hyperparameter adaptation and feature selection with respect to different model selection criteria. For the RVM model, the Gaussian radial based kernel function was used because of its popularity, high performance and general approximation ability. The sigest module supported by R language was used in this study which performs an automatic hyperparameter estimation to calculate an optimum sigma value for the Gaussian radial based function. According to Caputo et al. (2002), the "sigest" package is promising for estimating the range of values for the sigma parameter which could be used for obtaining good results. According to Caputo et al. (2002) any value between 0.1 and 0.9 quantile of $\|x - x'\|^2$ produce a good results. More detail about "sigest" is given over RCran web (http://cran.r-project.org/web/packages/kernlab/kernlab.pdf). The σ used for the analysis was 0.02. The RVM model produces 21 relevance vectors for best performance during the training and 9 vectors during the validation. Herein, the RVM involved very few relevant vectors for the regression to help minimise the possibility of overtraining and hence reduce the computational time. The R^2 for the rainfall during the training and validation were obtained as 0.35 and 0.30 respectively, while for the ETo, a higher training (0.77) and validation (0.72) were obtained.

3.3.2 Evaluation of the Bias Correction Schemes

The Taylor diagram (Taylor 2001) was employed herein to show the bias corrected datasets as compared to those obtained from the observed stations (Fig. 4). The perfect fit between model results and data was evaluated by using the circle mark in the x-axis, also called the reference point. In the case of a satisfactory agreement, simulated points will be closer to the reference point, indicating a better run of the model (Srivastava et al. 2014c). The result of the different
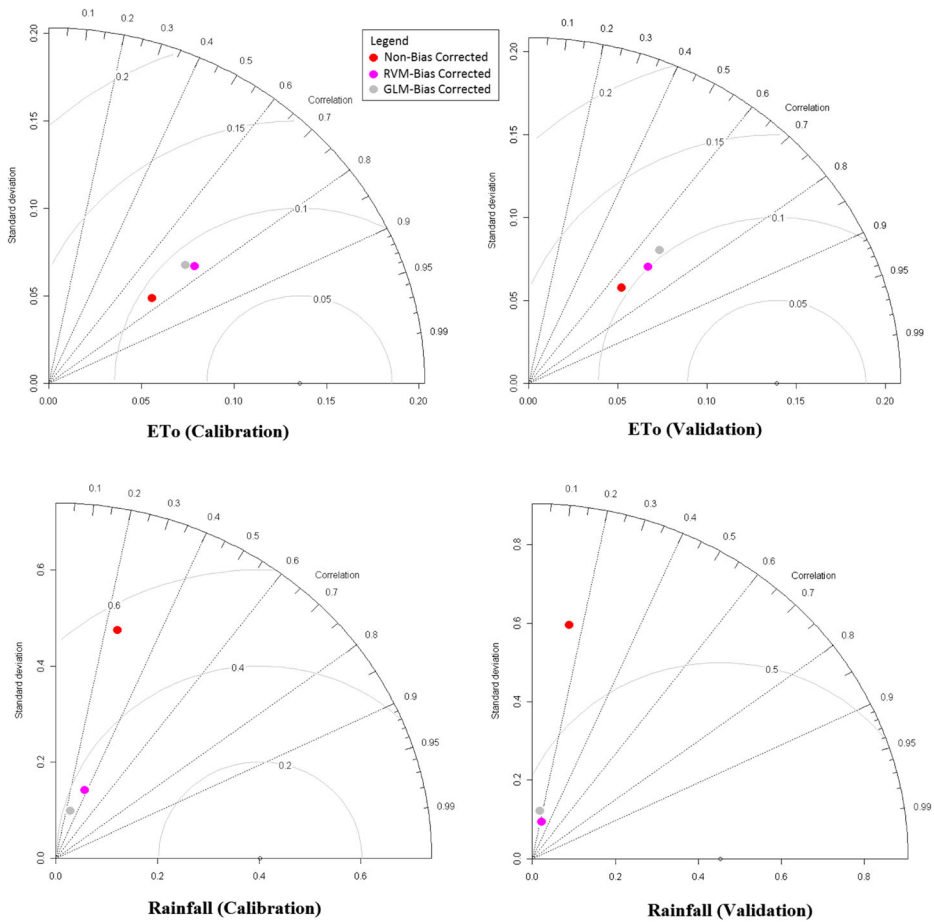
Fig. 4 Taylor performance plots for the bias and non-bias corrected rainfall and ETo

runs of the simulated model was determined by the values of the correlation (r), Centered Root Mean Square Difference ($RMSD$) and of the Standard Deviation (SD) of the modeled data shown on the two axis of the model, whereas correlation was represented by the quarter circle. In general, when the SD of the simulated data is higher than that of the observed values, an overestimation can be predicted and vice versa. The SD analysis showed that rainfall and ETo from WRF showed a higher overestimation than the measured datasets. Furthermore, a very small r; high SD and $RMSD$ were observed in-between the WRF and observed rainfall. On the other hand, in case of ETo, a better performance can be seen in Taylor plot. The analysis indicated a marginally higher $RMSD$, SD and lower r in case of GLM than RVM, imposing that probabilistic bias correction with RVM substantially improves the model's performance for both ETo and rainfall.

For a diagnostic performance evaluation of the model, four performance statistics- *RMSE, %Bias, d* and *r,* were estimated during the calibration (cal) and validation (val) to compare the observed with the WRF simulated non-bias and bias corrected datasets (Table 2). Looking at the distribution of the %Bias and (Fig. 5), the ETo was generally well simulated using the WRF model. The performance of RVM for ETo bias correction during the calibration/validation
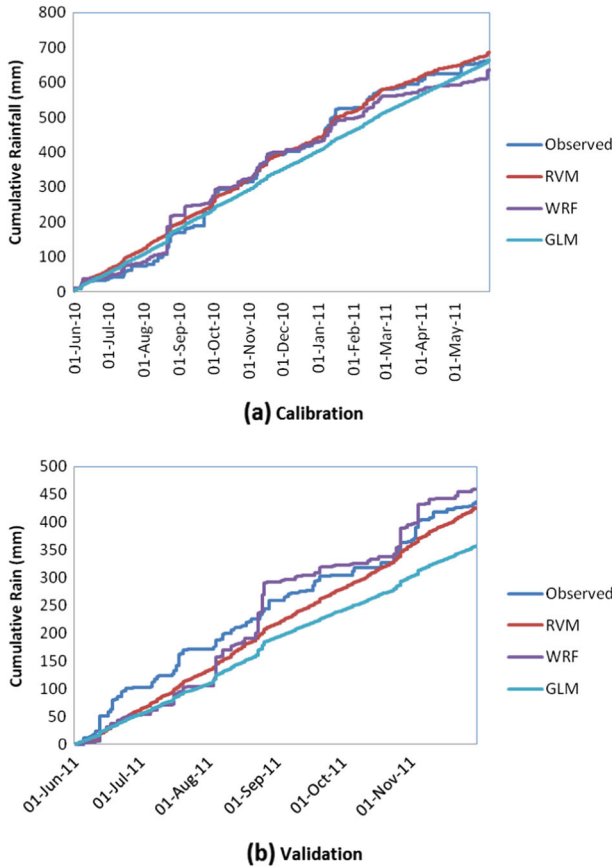
Fig. 5 (a-b) GLM and RVM calibration and validation cumulative time series plots for the rainfall

exhibited much higher r (cal=0.76; val=0.69) and d (cal=0.85; val=0.79) in comparison to the observed/WRF simulated data r (cal=0.75; val=0.68) and d (cal=0.76; val=0.72). The *RMSE* value for the RVM method during calibration and validation was 0.09 and 0.10 mm/hr respectively, while *%Bias* statistics were −1.1 and 3.9 respectively. This statistics indicate that the value of the *%Bias* was much higher in WRF simulated data when compared to the GLM and RVM.

Table 2 Performance statistics for WRF, GLM, and RVM for ETo and Rainfall

ETo					Rainfall				
Pairs	%Bias	RMSE	d	r	Pairs	%Bias	RMSE	d	r
Obs/WRF calibration	83.0	0.10	0.76	0.75	Obs/WRF calibration	4.5	0.55	0.41	0.25
Obs/WRF validation	82.0	0.11	0.72	0.68	Obs/WRF validation	−4.9	0.70	0.29	0.15
Obs/RVM calibration	−1.1	0.09	0.85	0.76	Obs/RVM calibration	−3.3	0.37	0.42	0.38
Obs/RVM validation	3.9	0.10	0.79	0.69	Obs/RVM validation	2.6	0.44	0.20	0.20
Obs/GLM calibration	–	0.10	0.84	0.75	Obs/GLM calibration	–	0.39	0.22	0.25
Obs/GLM validation	3.3	0.10	0.80	0.68	Obs/GLM validation	22.30	0.45	0.16	0.15

The RVM bias corrections of the ETo datasets showed an improved performance over GLM and WRF simulated data. Notably, the RVM bias correction of the rainfall exhibited similar values for *r* and *d* (*r* =0.20 and *d* =0.20) with lowest *%Bias* (2.6) and *RMSE* (0.44 mm/hr) during the validation. The *RMSE* values reported from the GLM bias correction for rainfall were 0.39 and 0.45 mm/hr during the calibration and validation respectively, while much higher values were obtained from the observed and WRF simulated rainfall. The *RMSE* and *%Bias* values compared to the Observed/WRF results indicated that the GLM did not perform very well for the bias correction in the case of rainfall. During the validation of rainfall, the GLM performance was poorer than that recorded by the RVM, indicating that RVM marginally outperformed the GLM in bias correction. Similar observations were also revealed by rainfall cumulative plots during calibration and validation (Fig. 5).

The overall analysis of GLM and RVM for Rainfall and ETo showed that the statistical bias correction of RVM was better than GLM during the both calibration and validation. This showed that the probabilistic bias correction scheme of RVM is more effective than point based bias correction of GLM. Hence, the probabilistic bias correction method could be a better choice than point-based bias correction of the data if employed with WRF downscaled hydro-meteorological variables using NCEP global reanalysis datasets.

4 Conclusions

This study provided for the first time a comprehensive model evaluation for new users who wish to apply the WRF model for hydrological modelling using the NCEP datasets. Moreover, it also provides a brief comparison of the performance of the RVM and GLM for bias correction in such models. The WRF numerical weather model was used because of its ability to downscale global reanalysis data to finer resolutions in space and time. The WRF bias correction process was found to generally improve the data quality in comparison with the original reanalysis datasets. In overall, GLM and RVM based bias correction improved the estimation of ETo and rainfall over the catchment. However, it was also observed that RVM outperformed GLM in bias correction in terms of all four statistical metrics *(%Bias, RMSE, d and r)*.

It was found that both the GLM and RVM indicated a good applicability in bias correction and are hence accurate methods to reduce the amount of error associated with WRF down-scaled data. Results from this study will potentially help in the retrieval of more accurate information from global downscaled data and will also help increase the efficiency of such data applicability in hydrological modelling. This work also provides hydrologists with valuable information on downscaled weather variables from global datasets and its applicability. However, further exploration of this potentially valuable data source by the hydro-meteorological community is recommended. The pattern obtained by precipitation with observed measurements indicates possibilities for further improvement with implication of data fusion techniques; therefore it will be attempted in future studies.

References

Abrahart R, See L (2007) Neural network modelling of non-linear hydrological relationships. Hydrol Earth Syst Sci 11:1563–1579

Allen RG, Pereira LS, Raes D, Smith M (1998) Crop evapotranspiration-guidelines for computing crop water requirements-FAO irrigation and drainage paper 56 FAO. Rome 300:6541

Borge R, Alexandrov V, José del Vas J, Lumbreras J, Rodríguez E (2008) A comprehensive sensitivity analysis of the WRF model for air quality applications over the Iberian Peninsula. Atmos Environ 42:8560–8574

Bringi V, Rico-Ramirez M, Thurai M (2011) Rainfall estimation with an operational polarimetric C-band radar in the United Kingdom: comparison with a gauge network and error analysis. J Hydrometeorol 12:935–954

Caldwell P, Chin H-NS, Bader DC, Bala G (2009) Evaluation of a WRF dynamical downscaling simulation over. Calif Clim Chang 95:499–521

Caputo B, Sim K, Furesjo F, Smola A (2002) Appearance-based Object Recognition using SVMs: Which Kernel Should I Use? In: Proc of NIPS workshop on Statistical methods for computational experiments in visual processing and computer vision, Whistler.

Chen F et al (2011) The integrated WRF/urban modelling system: development, evaluation, and applications to urban environmental problems. Int J Climatol 31:273–288

Chu PC, Fan C (1997) Sixth-order difference scheme for sigma coordinate ocean models. J Phys Oceanogr 27: 2064–2071

Draxl C, Hahmann AN, Pena Diaz A, Nissen JN, Giebel G (2010) Validation of boundary-layer winds from WRF mesoscale forecasts with applications to wind energy forecasting. In: 19th Symposium on Boundary Layers and Turbulence

Dudhia J (1989) Numerical study of convection observed during the winter monsoon experiment using a mesoscale two-dimensional model. J Atmos Sci 46:3077–3107

Ghosh S, Mujumdar P (2008) Statistical downscaling of GCM simulations to streamflow using relevance vector machine. Adv Water Resour 31:132–146

Gilliland EK, Rowe CM (2007) A comparison of cumulus parameterization schemes in the WRF model. In: Proceedings of the 87th AMS Annual Meeting & 21th Conference on Hydrology. p 2.16

Grell GA, Dudhia J, Stauffer DR (1994) A description of the fifth-generation Penn State/NCAR mesoscale model (MM5), NCAR TECHNICAL NOTE, NCAR/TN-398+STR, p128

Gutman G, Ignatov A (1998) The derivation of the green vegetation fraction from NOAA/AVHRR data for use in numerical weather prediction models. Int J Remote Sens 19:1533–1543

Hanna SR, Yang R (2001) Evaluations of mesoscale models' simulations of near-surface winds, temperature gradients, and mixing depths. J Appl Meteorol 40:1095–1104

Heikkila U, Sandvik A, Sorteberg A (2011) Dynamical downscaling of ERA-40 in complex terrain using the WRF regional climate model. Clim Dyn 37:1551–1564. doi:10.1007/s00382-010-0928-6

Heikkilä U, Sandvik A, Sorteberg A (2011) Dynamical downscaling of ERA-40 in complex terrain using the WRF regional climate model. Clim Dyn 37:1551–1564

Hong Y, Hsu KL, Sorooshian S, Gao X (2004) Precipitation estimation from remotely sensed imagery using an artificial neural network cloud classification system. J Appl Meteorol 43:1834–1853

Hu XM, Nielsen-Gammon JW, Zhang F (2010) Evaluation of three planetary boundary layer schemes in the WRF model. J Appl Meteorol Climatol 49:1831–1844

Ishak A, Remesan R, Srivastava P, Islam T, Han D (2013) Error correction modelling of wind speed through hydro-meteorological parameters and mesoscale model: a hybrid approach. Water Resour Manag 27:1–23. doi:10.1007/s11269-012-0130-1

Ishak AM, Srivastava PK, Gupta M, Islam T (2014) The development of numerical weather models-a review. Bull Environ Sci Res 3:15–20

Islam T, Rico-Ramirez MA, Han D, Srivastava PK, Ishak AM (2012a) Performance evaluation of the TRMM precipitation estimation using ground-based radars from the GPM validation network. J Atmos Sol Terr Phys 77:194–208

Islam T, Rico-Ramirez MA, Han D, Srivastava PK (2012b) A Joss–Waldvogel disdrometer derived rainfall estimation study by collocated tipping bucket and rapid response rain gauges. Atmos Sci Lett 13:139–150

Islam T, Rico-Ramirez MA, Han D, Bray M, Srivastava PK (2013) Fuzzy logic based melting layer recognition from 3 GHz dual polarization radar: appraisal with NWP model and radio sounding observations. Theor Appl Climatol 112:317–338

Islam T, Srivastava PK, Gupta M, Zhu X, Mukherjee S (2014) Computational Intelligence Techniques in Earth and Environmental Sciences. Springer, Netherlands

Johnson RA, Wichern DW (2002) Applied multivariate statistical analysis, vol 4. Prentice hall Upper Saddle River, NJ

Legates DR, McCabe GJ Jr (1999) Evaluating the use of "goodness-of-fit" measures in hydrologic and hydroclimatic model validation. Water Resour Res 35:233–241

Liolios KA, Moutsopoulos KN, Tsihrintzis VA (2014) Comparative modeling of HSF constructed wetland performance with and without evapotranspiration and rainfall. Environ Process 1:171–186

Lo JCF, Yang ZL, Pielke RA (2008) Assessment of three dynamical climate downscaling methods using the Weather Research and Forecasting (WRF) model. J Geophys Res: Atmos (1984–2012) 113

Lorenc AC (1986) Analysis methods for numerical weather prediction. Q J R Meteorol Soc 112:1177–1194

Mahmood R, Hubbard KG (2005) Assessing bias in evapotranspiration and soil moisture estimates due to the use of modeled solar radiation and dew point temperature data. Agric For Meteorol 130:71–84

McCullagh P, Nelder JA (1989) Generalized linear models, Chapman and Hall/CRC press. ISBN-13: 978–0412317606, p 532

Mlawer EJ, Taubman SJ, Brown PD, Iacono MJ, Clough SA (1997) Radiative transfer for inhomogeneous atmospheres: RRTM, a validated correlated-k model for the longwave. J Geophys Res 102:16663–16616, 16682

Monteith J (1965) Evaporation and environment. pp 205–234

Penman H (1956) Estimating evaporation. Trans Am Geophys Union 37:43–50

Petropoulos GP, Carlson TN, Griffiths H (eds) (2013) Turbulent Fluxes of Heat and Moisture at the Earth's Land Surface: Importance, Controlling Parameters and Conventional Measurement, Chapter 1, pages 3–28, in "Remote Sensing of Energy Fluxes and Soil Moisture Content", by G.P. Petropoulos, Taylor and Francis, ISBN: 978-1-4665-0578-0. CRC Press

Piani C, Haerter JO, Coppola E (2010a) Statistical bias correction for daily precipitation in regional climate models over. Eur Theor Appl Climatol 99:187–192. doi:10.1007/s00704-009-0134-9

Piani C, Weedon G, Best M, Gomes S, Viterbo P, Hagemann S, Haerter J (2010b) Statistical bias correction of global simulated daily precipitation and temperature for the application of hydrological models. J Hydrol 395:199–215

Price K, Purucker T, Andersen T, Knightes C, Cooter E, Otte T (2012) Comparison of Spatial and Temporal Rainfall Characteristics of WRF-Simulated Precipitation to gauge and radar observations. In: AGU Fall Meeting Abstracts. p 1295

Ritter B, Geleyn J-F (1992) A comprehensive radiation scheme for numerical weather prediction models with potential applications in climate simulations. Mon Weather Rev 120:303–325

Schoof JT, Pryor S (2001) Downscaling temperature and precipitation: a comparison of regression-based methods and artificial neural networks. Int J Climatol 21:773–790

Skamarock WC, Klemp JB, Dudhia J, Gill DO, Barker DM, Wang W, Powers JG (2005) A description of the advanced research WRF version 2, (No. NCAR/TN-468+ STR). National Center for Atmospheric Research Boulder Co Mesoscale and Microscale Meteorology Divison

Srivastava PK (2013) Soil Moisture Estimation from SMOS Satellite and Mesoscale Model for Hydrological Applications. PhD Thesis, University of Bristol, Bristol, United Kingdom

Srivastava PK, Han D, Ramirez MR, Islam T (2013a) Machine learning techniques for downscaling SMOS satellite soil moisture using MODIS land surface temperature for hydrological application. Water Resour Manag 27:3127–3144

Srivastava PK, Han D, Rico-Ramirez MA, Al-Shrafany D, Islam T (2013b) Data fusion techniques for improving soil moisture deficit using SMOS satellite and WRF-NOAH land surface model. Water Resour Manag 27:5069–5087

Srivastava PK, Han D, Rico-Ramirez MA, Islam T (2013c) Appraisal of SMOS soil moisture at a catchment scale in a temperate maritime climate. J Hydrol 498:292–304

Srivastava PK, Han D, Rico Ramirez MA, Islam T (2013d) Comparative assessment of evapotranspiration derived from NCEP and ECMWF global datasets through weather research and forecasting model. Atmos Sci Lett 14:118–125

Srivastava PK, Han D, Rico-Ramirez MA, Bray M, Islam T, Gupta M, Dai Q (2014a) Estimation of land surface temperature from atmospherically corrected LANDSAT TM image using 6S and NCEP global reanalysis product. Environ Earth Sci 72:5183–5196

Srivastava PK, Han D, Rico-Ramirez MA, Islam T (2014b) Sensitivity and uncertainty analysis of mesoscale model downscaled hydro-meteorological variables for discharge prediction. Hydrol Process 28:4419–4432. doi:10.1002/hyp.9946

Srivastava PK, Han D, Rico-Ramirez MA, O'Neill P, Islam T, Gupta M (2014c) Assessment of SMOS soil moisture retrieval parameters using tau–omega algorithms for soil moisture deficit estimation. J Hydrol 519: 574–587

Srivastava PK, Mukherjee S, Gupta M, Islam T (2014d) Remote Sensing Applications in Environmental Research. Springer, Verlag

Taylor KE (2001) Summarizing multiple aspects of model performance in a single diagram. J Geophys Res: Atmos (1984–2012) 106:7183–7192

Tipping ME (2001) Sparse Bayesian learning and the relevance vector machine. J Mach Learn Res 1:211–244

Trigo RM, Palutikof JP (2001) Precipitation scenarios over Iberia: a comparison between direct GCM output and different downscaling techniques. J Clim 14:4422–4446

Vaidya S, Singh S (2000) Applying the Betts-Miller-Janjic scheme of convection in prediction of the Indian monsoon. Weather Forecast 15: 349–356

Weichert A, Bürger G (1998) Linear versus nonlinear techniques in downscaling. Clim Res 10:83–93

Willmott CJ et al (1985) Statistics for the evaluation and comparison of models. J Geophys Res 90:8995–9005

Zhong X (1996) Additive semi-implicit Runge–Kutta methods for computing high-speed nonequilibrium reactive flows. J Comput Phys 128: 19–31